

# The Interactions Between Oxide Film Inclusions and Inoculation Particles $\text{TiB}_2$ in Aluminum Melt



JIAWEI YANG, SARINA BAO, SHAHID AKHTAR, and YANJUN LI

In this work, a systematic study on the interactions between aluminum oxide films and  $\text{TiB}_2$  grain refiner particles and their effect on grain refinement behavior have been conducted. Oxide films were introduced into a commercial purity aluminum melt by adding AA 6061 alloy chips while the grain refiner particles were introduced by adding Al-3Ti-1B master alloy. Strong sedimentation of  $\text{TiB}_2$  grain refiner particles was observed in aluminum melt without chip addition during long-time settling. Most of the  $\text{TiB}_2$  particles were settled and accumulated at the bottom of crucible. In contrast, the sedimentation of  $\text{TiB}_2$  particles is much less in the melt with the addition of oxide films. A large fraction of  $\text{TiB}_2$  particles were found to be adhered to the oxide films located at the top part of the crucible, which inhibited the sedimentation of grain refiner particles. TP-1 type tests were also done to study the grain refinement efficiency of Al-3Ti-1B master alloy under different melt cleanliness and settling time. It is found that sedimentation of  $\text{TiB}_2$  particles greatly reduces the grain refinement efficiency. The introduction of oxide films seems to slightly alleviate the fading effect. This is owing to the strong adherence between the oxide films and  $\text{TiB}_2$  particles, which leads to a retardation of particle sedimentation.

<https://doi.org/10.1007/s11663-021-02160-3>  
© The Author(s) 2021

## I. INTRODUCTION

GRAIN refiners are commonly added to the aluminum alloys in order to achieve a fine equiaxed grain structure, which improves the mechanical properties of final products. Al-Ti-B and Al-Ti-C master alloys are the two most commonly used grain refiners in the aluminum industry.<sup>[1-4]</sup> The addition of the master alloys can provide a high number density of potent heterogeneous nucleation sites for aluminum grains like  $\text{TiB}_2$  and TiC particles. The grain refinement mechanism has been extensively studied in the past decades through both experiments and theoretical modeling works.<sup>[1-10]</sup>

The grain refinement efficiency is closely related to the nucleation potency of inoculant particles, the alloy chemistry in terms of grain growth restriction factors, and the solidification conditions including cooling rate and temperature gradient. Under the same solidification conditions, the grain refinement of a certain alloy will be

determined by the number density, size, and size distribution of inoculant particles in the melt. It is well known that the effectiveness of the grain refiners decays with increasing holding time of inoculated melt before casting, which is the so-called fading effect.<sup>[11-13]</sup> One of the major reasons for such fading effect of Al-Ti-B master alloys is ascribed to the settling and agglomeration of  $\text{TiB}_2$  particles. The settling makes grain refiner particles less uniformly distributed in the melt and the agglomeration makes a decrease in the number density of the potential nucleation particles. Furthermore, the agglomerated large grain refiner cluster is also counted as inclusions, which reduces the melt quality.

Schaffer *et al.*<sup>[13]</sup> studied the settling and fading behavior of three different Al-Ti-B master alloys, namely Al-5Ti-1B, Hydloy (Al-1.2Ti-0.5B), and TiBloy (Al-1.6Ti-1.4B). It was found that settling of grain refiner particles was much faster than Stokes' law predicted. This has been attributed to the agglomeration of grain refiner particles, which has a higher settling rate than the individual ones. They also observed that the massive  $\text{TiB}_2$  particles were pushed to the grain boundaries after solidification. Similar phenomenon has also been observed by Kumar *et al.*,<sup>[14]</sup> who studied the settling behavior of  $\text{TiB}_2$ , TiC,  $\text{AlB}_2$ , and  $\text{TiAl}_3$  in liquid Al. They found that the settling of grain refiner particles is through the self-agglomeration of particles. At higher addition levels, the settling of grain refiner particles is faster.

JIAWEI YANG and YANJUN LI are with the Norwegian University of Science and Technology, Trondheim, 7491, Norway. Contact e-mail: [jiawei.yang@ntnu.no](mailto:jiawei.yang@ntnu.no) SARINA BAO is with the SINTEF Industry, Trondheim, 7465, Norway SHAHID AKHTAR is with the Research and Development Karmøy, Norsk Hydro, Håvik, 4265, Norway.

Manuscript submitted on January 1, 2021; accepted March 23, 2021.

Article published online May 20, 2021.

The inclusions in aluminum melt also tend to agglomerate, similar to grain refiner particles. Tian *et al.*<sup>[15]</sup> investigated the settling of multisided clusters of alumina particles in liquid Al. The settling started right after the stirring was stopped. Alumina particle clusters were often observed together with entrained aluminum oxide films. Badowski *et al.*<sup>[16]</sup> studied the settling and sedimentation behavior of alumina particles under the influence of melt flow in a crucible by both modeling and experiments. Their result showed that thermal and natural convections had a strong influence on the particle motion in the melt, *i.e.*, the settling of the particle is dependent on the melt flow, especially when the melts contain large portions of Al<sub>2</sub>O<sub>3</sub> films.

It is always important to remove the inclusions from the aluminum melt in order to improve the metal quality of aluminum products. There are three major contaminations in the aluminum melt: gas, non-metallic inclusions, and alkali and alkaline earth metals.<sup>[17]</sup> Melt filtration by using ceramic foam filters (CFF) has been widely used in industry to remove the inclusions in aluminum melt, including mostly oxide, carbide, nitride, and boride. However, the addition of grain refiners has the effect of reducing the filtration efficiency of aluminum melt with high inclusion loads.<sup>[18–22]</sup> A major explanation for this has been based on the inclusion bridge mechanism, where inclusions form “bridge” in the ceramic cell, and thus increase filtration efficiency.<sup>[19,20]</sup> The addition of grain refiner particles in the melt, like TiB<sub>2</sub> and TiC, was supposed to prevent the formation of the bridge or destroy the inclusion bridge, which causes a reduction in filtration efficiency.<sup>[19,20]</sup> But, how and why the grain refiner particles destroy the bridge is still unclear. Experimental evidence to support this inclusion bridge theory have been few.

In a recent work by the present authors, it has been found that grain refiner particles TiB<sub>2</sub> and TiC particles have the influence of increasing the wettability between Al melt and alumina substrate during wetting tests.<sup>[23]</sup> It is shown that the grain refiner particles tend to adhere to the oxide film covering the aluminum droplet during wetting test. Based on the results, we suggested that the improved wetting between aluminum melt and alumina substrate may not be the main reason for the reduction of filtration efficiency, but the interaction between grain refiners and inclusions may be a key factor. Therefore, a systematic study of the interactions between grain refiners and inclusions is necessary.

The present work is aimed at an in-depth understanding between the inclusions and grain refiner during settling. The influence of inclusions on the fading effect and grain refinement efficiency of grain refiners is also

investigated. This may further help to reveal the underlying mechanism for the reduced filtration efficiency by grain refiners in aluminum melt.

## II. EXPERIMENTAL

### A. Materials

The experimental materials used in this work include commercial purity aluminum (CP-Al), commercial Al-3Ti-1B master alloy, and AA6061 alloy chips with dimensions of 1 mm × 4 mm × 50 mm provided by Hydro Aluminum (Sunndalsøra, Norway). The chemical compositions of CP-Al and AA 6061 chips are listed in Table I. The chips were used to introduce inclusions in the aluminum melt, mostly in the form of the oxide film. Since the 6061 alloy contains a relatively high Mg content, it is easy to form Mg-rich aluminum oxides and spinel film in the melt, which are easier to be distinguished during characterization of solidification structures.<sup>[24]</sup> In addition, aluminum oxide-cement powders (Alfa Aesar, Haverhill, Massachusetts, United States) were used as extra inclusions source for the settling experiment to compare with the only oxide films case. The chemical compositions of the ceramic powders are 95 wt pct Al<sub>2</sub>O<sub>3</sub> and 5 wt pct SiO<sub>2</sub>. The particle size of the powders approximately is in the range of 0.5 to 300 μm.

### B. Settlement Test

Two types of melt, CP-Al and a mixture of CP-Al and 20 wt pct AA6061 chips and 1 wt pct of aluminum oxide-cement powder were used in the present work. 1 kg of CP-Al was melted in an alumina crucible at 750 °C in a muffin furnace. For the melt with chips addition, 800 g of CP-Al was first melted in a muffin furnace, thereafter, 200 g chips were introduced into the melt aided by mechanical stirring. After the chips were completely melted, 1 wt pct aluminum oxide-cement powders which were pre-treated at 800 °C for 15 minutes were introduced into the melt by mechanical stirring. Al-3Ti-1B master alloy was added for both melts with an addition level of 10 g/kg, where a stirring was conducted to make sure a full dispersion of the grain refiner particles. The melts were air-cooled in the crucibles right after the addition of grain refiners or after 4 hours of holding at 750 °C in the furnace, as listed in Table II. The solidified ingots of the settling tests were vertically cut, ground, polished, and examined by Optical Microscopy (OM) (MEF4M, LEICA,

Table I. Chemical Compositions of CP-Al and AA 6061 Alloy in wt pct

Compositions	Si	Fe	Cu	Mn	Mg	Al
CP-Al	0.06	0.06	0.001	0.001	0.001	balance
AA 6061	0.4 to 0.8	0.7	0.15 to 0.4	0.15	0.08 to 0.12	balance

**Table II. Experimental Overview of the Settlement Test**

Sample	Metal Used	Settling of Melt
A	CP-Al	no
B	CP-Al	4 hours
C	CP-Al+ chips + powder	no
D	CP-Al+ chips + powder	4 hours

Wetzlar, Germany) and Scanning Electron Microscopy (SEM) (SUPRA 55-VP, Zeiss, Oberkochen, Germany) with an Energy Dispersive X-ray Spectroscopy (Octane, EDAX, Mahwah, USA). An accelerating voltage of 15 kV and a working distance of 10 to 15 mm were applied in the SEM observation.

### C. TP-1 Type Test

TP-1 type tests were made for each melt. A pre-heated (same temperature as the melt, ~750 °C) boron nitride-coated TP-1 type steel crucibles with a wall thickness of 2 mm, a height of 30 mm, and an outer diameter of 33/23 mm were used for aluminum sampling in present work. Liquid aluminum was taken out from the upper part of the crucible with approximately 2 cm distance to the top of the melt. After the sampling of the melt, the crucible was covered by the insulation materials at both top and bottom during the solidification process. The major difference between TP-1 type test<sup>[25]</sup> and standard TP-1 test<sup>[26]</sup> is that casting crucibles of different dimensions and different cooling conditions are used. The cooling curve is measured by a well-calibrated K-type thermocouple, which was inserted in the central region of the crucible. A temperature logger with a frequency of 50 Hz (corresponding to 0.02 seconds per measurement) was used to measure and log the cooling curve. The solidified sample ingots were all cut, mechanically polished, and then anodized with 95 wt pct H<sub>2</sub>O + 5 wt pct HBF<sub>4</sub> solution at 20 V with 90 seconds for microstructure characterization by OM. The line intercept method was used to determine the average grain size of grains at the central regions of the ingot.

## III. RESULTS

### A. Settling of Grain Refiner Particles in CP-Al

The total height of the solidified ingots in the settlement tests is approximately 4.5 cm for all samples. The solidification microstructures of the sample without holding time in the longitudinal section, at the top, middle, and bottom are shown in Figures 1(a) through (c), respectively. It can be seen that a large fraction of white phases has precipitated along grain boundaries at all height. With a magnified image in Figure 1(d), this white phase at the top height is identified as Al<sub>3</sub>Fe by a careful EDS examination. Besides the intermetallic phase, TiB<sub>2</sub> particle clusters can also be found in the whole sample. Figure 1(e) shows a typical TiB<sub>2</sub> cluster found in the middle section as marked in Figure 1(b). Figure 1(f) shows a typical grain boundary in the

bottom, where the TiB<sub>2</sub> particles are agglomerated together with Al<sub>3</sub>Fe intermetallic particles. The fraction of TiB<sub>2</sub> clusters in the bottom is obviously larger than that in the middle and top part of the ingot, showing that settling of TiB<sub>2</sub> particles has occurred during the slow solidification process.

Figure 2 shows the microstructure of Sample B solidified after 4 hours of holding at 750 °C. Similar to sample A in Figure 1, a large fraction of the white Al<sub>3</sub>Fe intermetallic particles can be seen along the grain boundaries (Figures 2(a) and (b)). In contrast to Sample A, no grain refiner particles can be observed at the top of the ingot in Sample B after 4 hours of settling. Furthermore, the grain boundaries at the bottom part of sample B are thicker (Figure 2(c)) in comparison to the top (Figure 2(a)) and middle (Figure 2(b)) parts. A large amount of TiB<sub>2</sub> particles in addition to the Al<sub>3</sub>Fe intermetallic particles are distributed along the grain boundaries, as shown in Figure 2(d). This indicates that most of the TiB<sub>2</sub> particles in the melt have agglomerated and sedimented in the bottom of the ingot during the 4 hours of holding and settling.

### B. Influence of Oxides on the Settling of Grain Refiner Particles

Figures 3(a) through (c) show the solidification structure of inoculated CP-Al with the addition of chips and oxide powders without holding time. In addition to the white powder structure along the grain boundaries, some black films can be found at the top of the ingot. EDS measurement confirms that these black oxide films contain 15 wt pct Mg in addition to 48 wt pct Al and 37 wt pct O, implying that the oxide films are most likely AlMgO films or spinel as shown in Figure 4. Furthermore, the introduced Al<sub>2</sub>O<sub>3</sub> particles are also found both in the top and bottom of the ingot and marked in Figure 3. TiB<sub>2</sub> particles are agglomerated (Figure 3(d)) along the oxide films distributing (Figure 3(a)) at the top of the ingot. A large number of TiB<sub>2</sub> particles (Figure 3(e)) can also be seen along the grain boundaries (Figure 3(e)) together with Al-Fe-Si intermetallic particles in the middle part, besides some TiB<sub>2</sub> clusters particles in the intragranular regions. Figure 3(f) shows a magnified area around a black alumina particle in the bottom section, where no obvious adherence between TiB<sub>2</sub> particles and the introduced alumina particles can be seen.

The solidification structure of the ingot after 4 hours of holding at 750 °C is shown in Figure 5. A large number of TiB<sub>2</sub> particles that agglomerate together with oxide films can still be observed at the top part of the ingot (Figures 5(a) and (d)). Figures 5(b) and (e) show the structure in the middle part of the ingot. No large oxide films or alumina particles can be observed. However, the grain boundary white phases look thicker than in the top part of the ingot. A typical triple junction of grain boundaries with the white phases is shown in Figure 5(e). As can be seen, it is decorated with Al-Fe-Si particles and agglomerated TiB<sub>2</sub> particles. Interestingly, the bottom part of the ingot (Figures 5(c) and (f)) does not appear as much thicker grain boundaries than in

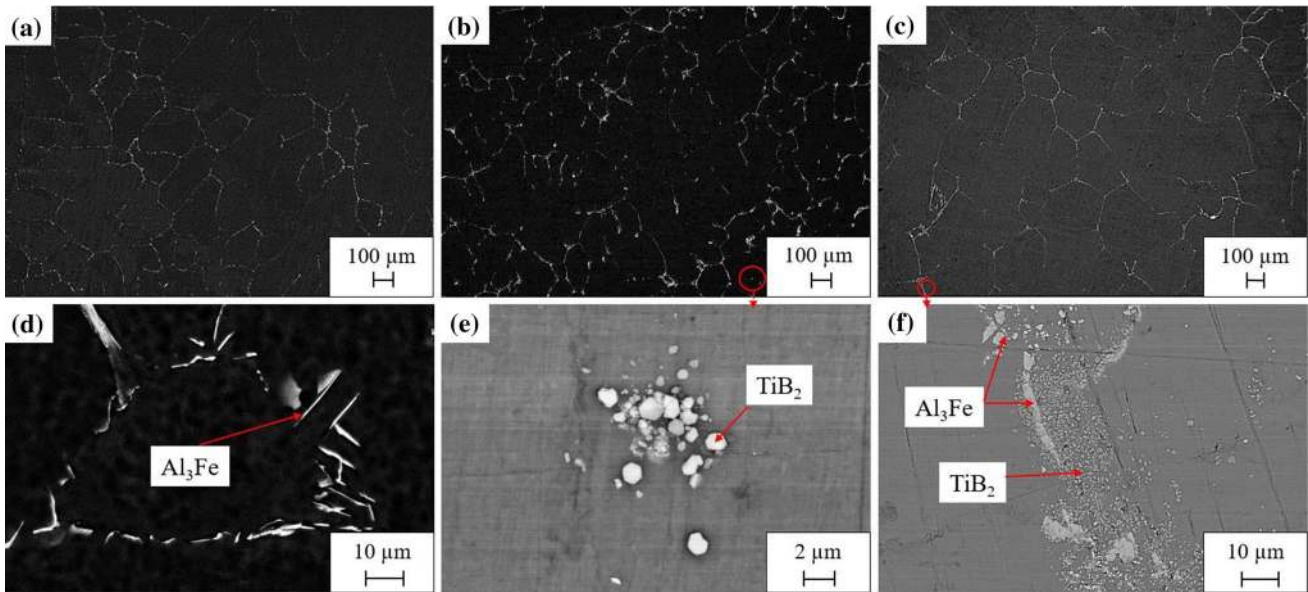


Fig. 1—Microstructure of inoculated CP-Al (Sample A) which solidified immediately after the grain refiners were added at 750 °C, in the top (*a*, *d*), middle (*b*, *e*), and bottom sections (*c*, *f*) of the ingot. (*d*) Typical Al<sub>3</sub>Fe intermetallic phase precipitated along the grain boundaries. (*e*) Magnified picture of TiB<sub>2</sub> cluster in (*b*). (*f*) Typical grain boundary in the bottom section where TiB<sub>2</sub> particles agglomerate together with Al<sub>3</sub>Fe phase along the grain boundary.

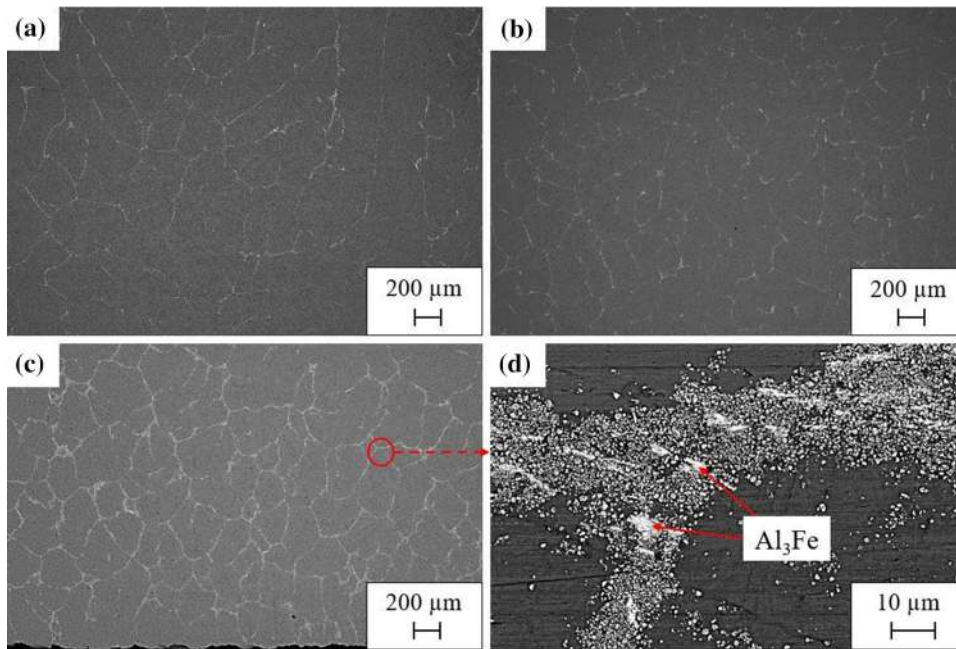


Fig. 2—Solidification structure of inoculated CP-Al (Sample B) after 4 h of settling at 750 °C in the top (*a*), middle (*b*), and bottom sections (*c*) of the crucible. (*d*) shows the magnified area in (*c*), where massive TiB<sub>2</sub> particles agglomerate along the grain boundaries in the bottom section.

middle (Figure 5(b)) part as sample B does. The amount of TiB<sub>2</sub> sedimented at the bottom is significantly reduced in comparison to sample B, implying that the introduction of oxide films has reduced the sedimentation of TiB<sub>2</sub> particles.

The optical microscopy images of the bottom sections of all samples are summarized in Figure 6 to compare the sedimentation of TiB<sub>2</sub> particles. Sample B (Figure 6(b)) has much thicker and clear grain boundaries than Sample A (Figure 6(a)), indicating the increase of

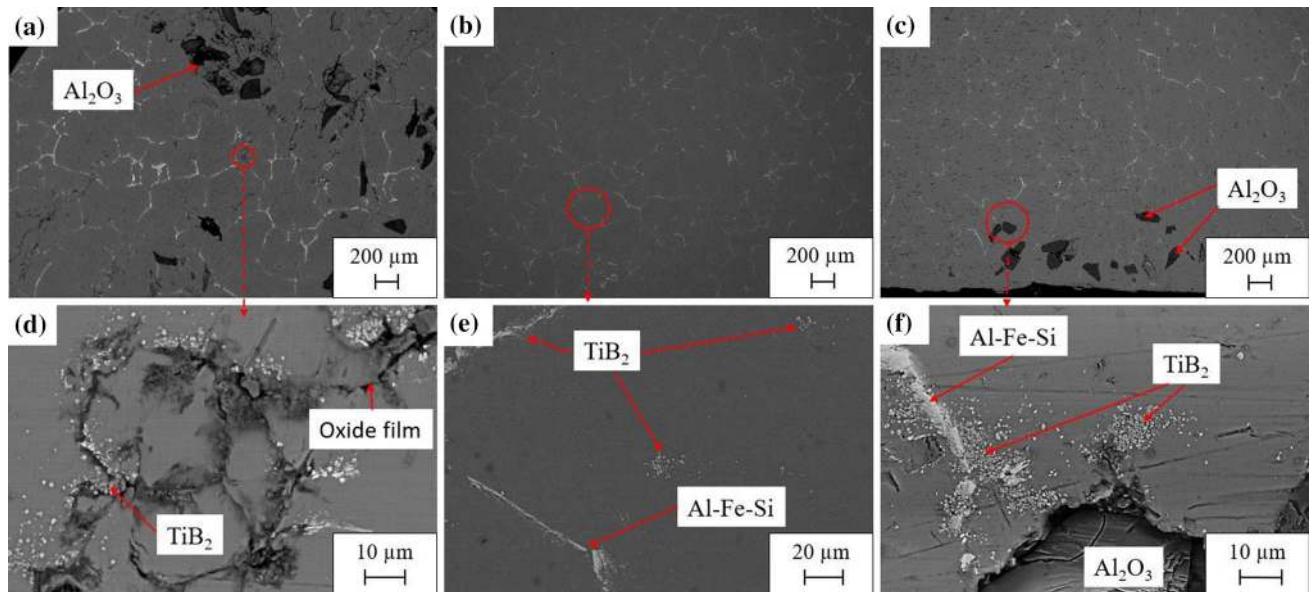


Fig. 3—(a) through (c) Solidification microstructure of inoculated CP-Al (Sample C) with the addition of chips and oxide powders solidified immediately after the grain refiners are added, in the top (a, d); middle (b, e); and bottom (c, f) sections of the ingot. (d) through (f) show the magnified area in a), b), and c), respectively.

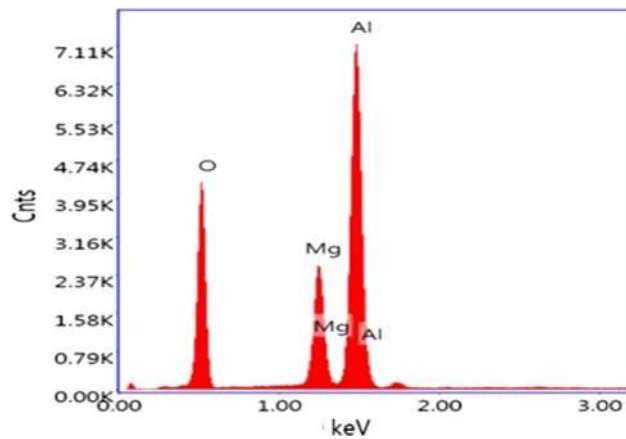


Fig. 4—EDS result of a measured black oxide film which contains O, Mg, and Al, suggesting these black films are most likely AlMgO films or spinel.

agglomeration of  $\text{TiB}_2$  particles along the grain boundaries with increasing holding time. Such thick grain boundaries decorated with  $\text{TiB}_2$  particles become less with increasing distance from the bottom. At locations with a height of 2.6 mm, the grain boundaries are becoming cleaner, indicating that most of the  $\text{TiB}_2$  particles have sedimented in the bottom layer of the ingot. As a big contrast, the difference in the appearance of the grain boundaries in samples with additions of chips and alumina, Samples C and D, is much less than that in between Sample A and B. As shown in Figure 6(d), even after 4 hours of holding at 750 °C, there is only a thin layer with a thickness less than 0.5 mm at bottom of sample D, containing thick grain boundaries like Sample B. It further confirms that the sedimentation and agglomeration of  $\text{TiB}_2$  particles are significantly reduced by the introduction of oxide films.

### C. Effect of Settling on Grain Refinement

Figures 7(a) and (b) show the grain structure of TP-1 type test ingots of CP-Al cast immediately after grain refiner addition, and after 4 hours of holding at 750 °C, corresponding to sample A and B, respectively. As can be seen, equiaxed grain structure has been achieved in both samples. However, the grain size of the sample after four hours of holding is significantly larger than that without holding. The average grain size is 481  $\mu\text{m}$  for Sample A and 627  $\mu\text{m}$  for the Sample B. This indicates that the grain refinement efficiency reduces over holding time, owing to the settling and agglomeration of grain refiner particles in the bottom of the crucible.

Figure 7(c) shows the measured cooling curves of TP-1 test samples during solidification. The initial cooling rate for Sample A and B during solidification is measured as approximately 1.8 K/s. In both cooling curves, recalescence can be clearly observed. From the temperatures for recalescence occurring, it can be clearly seen that the maximum nucleation undercooling  $\Delta T_{n, \text{max}}$  of sample B is larger than that of A, indicating that the number density of effective inoculant particles in the former sample is less than in the latter one. It further confirms that 4 hours of holding of the melt at 750 °C has caused a strong decrease of  $\text{TiB}_2$  particles in the top part of the melt in the crucible, due to the sedimentation of  $\text{TiB}_2$  particles to the bottom of the crucible. This is consistent with the observations in Figures 6(a) and (b).

Figures 8(a) and (b) show the grain structure of TP-1 test ingots of CP-Al melt with the addition of chips and alumina inclusions cast immediately after grain refiner addition and after 4 hours of holding at 750 °C, corresponding to samples C and D with an initial measured cooling rate of  $\sim 1.5$  K/s. As can be seen, both

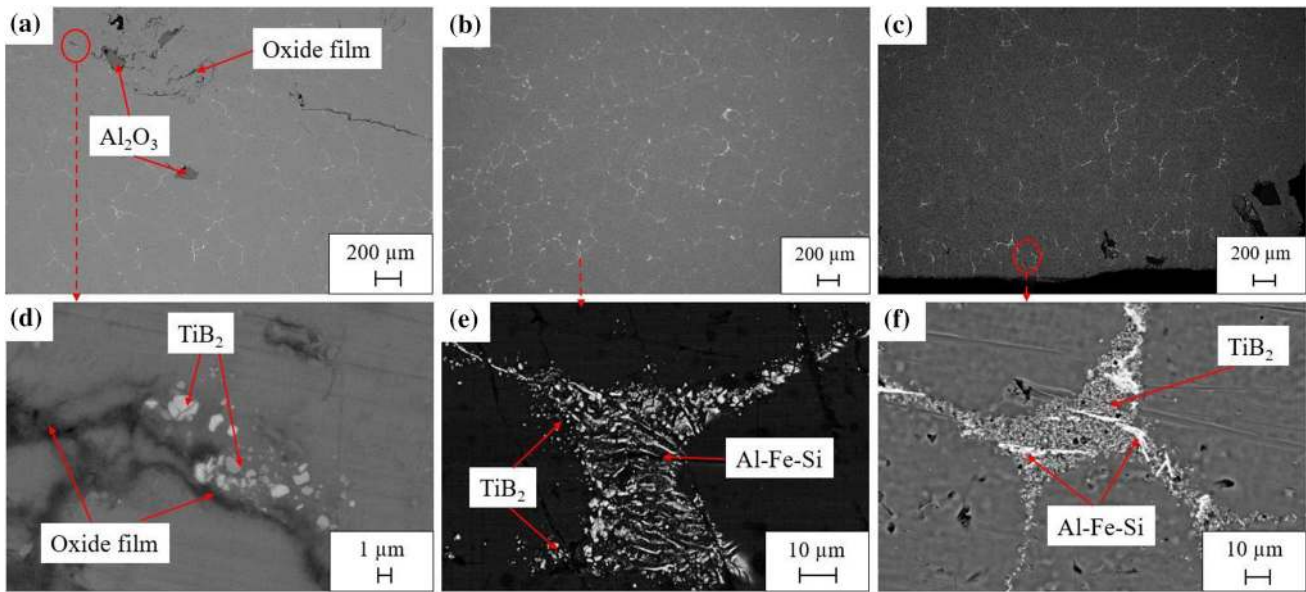


Fig. 5—(a) through (c) The solidified microstructure of inoculated aluminum melt (Sample D) with the addition of chips and oxide powders after 4 hours of settling at 750 deg, in the top (a), middle (b), and bottom (c) sections, respectively. (d) through (f) show the magnified image of the corresponding area in (a) through (c).

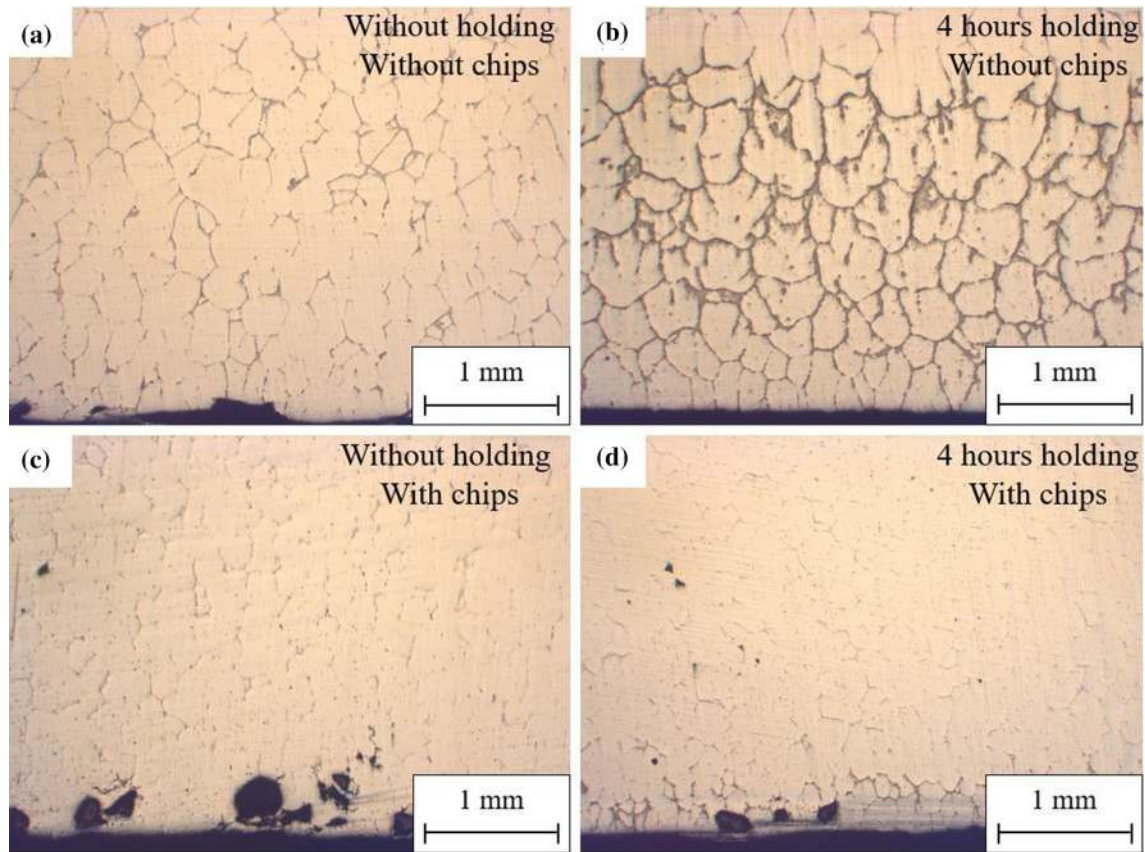


Fig. 6—Grain boundary morphology in the bottom sections of all four samples, (a) sample A, (b) sample B, (c) Sample C, and (d) sample D.

samples show equiaxed grain structure. However, the grains in sample C are smaller and more uniform than sample D. The average grain size of samples C and D

are measured as 236 and 366  $\mu\text{m}$ , respectively, indicating that a long-time holding of the melt with high inclusion load also causes a decrease of grain refinement

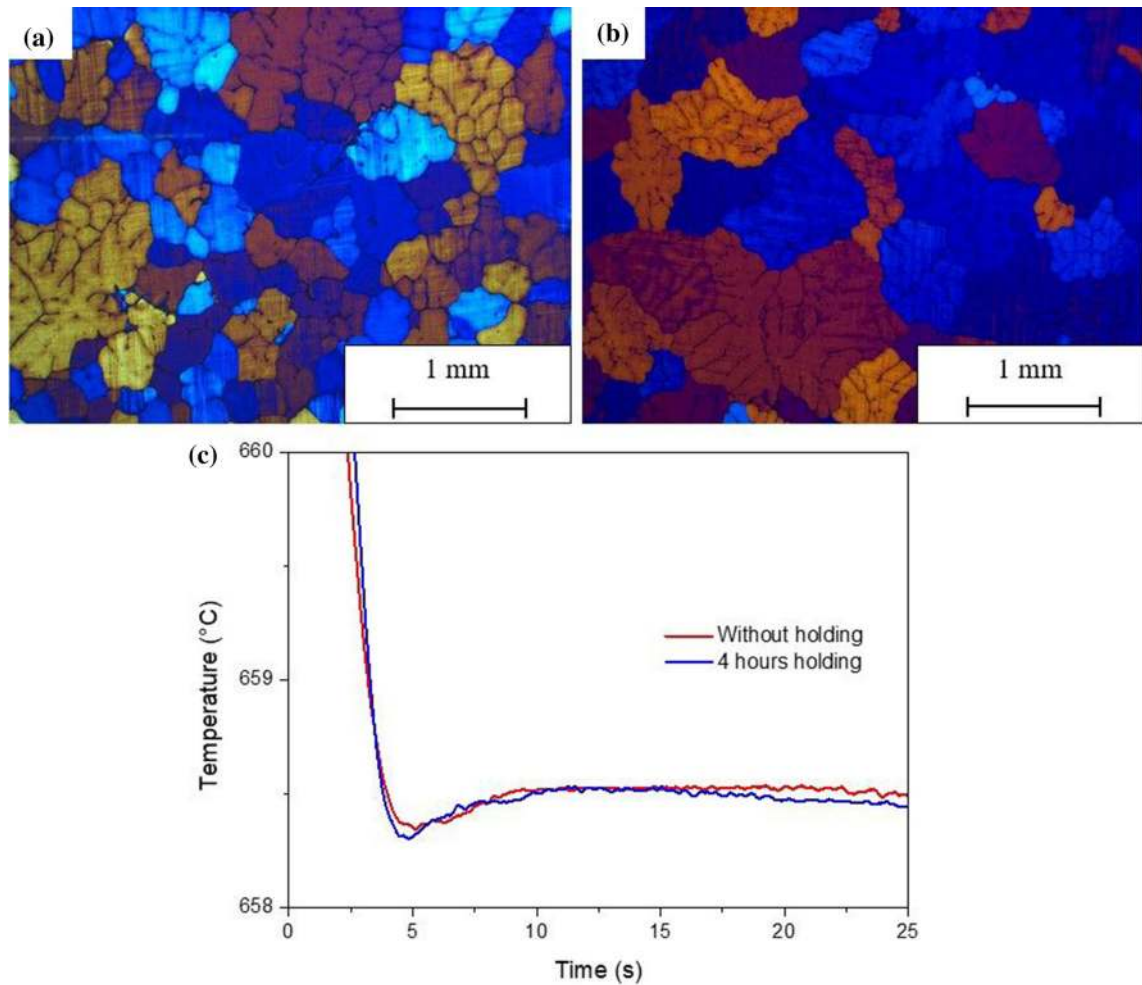


Fig. 7—Solidification structure and cooling curve for sample A and B from TP-1 type test. (a) Solidified structure after anodizing of CP-Al with 10 g/kg Al-3Ti-1B with no holding time. (b) solidified structure after anodizing of CP-Al with 10 g/kg Al-3Ti-1B with 4 hours of holding time. (c) The cooling curve of samples A and B.

efficiency. However, this decrease in grain refinement efficiency looks less significant than that of CP-Al melts without inclusions.

The cooling curves and the corresponding first derivatives,  $dT/dt$ , of Samples C and D are shown in Figure 8(c). The nucleation temperature can be determined from the  $dT/dt$  curve, where the cooling rate curve shows a sharp increase. From the  $dT/dt$  curves, it seems that the nucleation start temperature of sample C is slightly higher than sample D, even though the lowest point before recalescence is similar. From the  $dT/dt$  curves, it is difficult to detect the difference in nucleation start temperature of the two samples. This can be due to the ultrahigh addition level of grain refiners in this study, 10 g/kg, which is much higher than the normal addition level, 0.5 to 2.0 g/kg. It is worth of mention that the grain size of the ingots with chip additions is much smaller than that of the CP-Al samples without chip addition (Figure 7). This can be attributed to the alloying effect of adding AA 6061 chips that contain alloy elements such as Si, Mg, and Cu. With these elements in the alloy, the grain growth restriction factor,  $Q$ , of the alloy is substantially higher than CP-Al.

## IV. DISCUSSION

### A. Agglomeration and Settling of $TiB_2$

It is well known that grain refiner particles,  $TiB_2$ , tend to agglomerate and sediment in aluminum melt owing to the higher density of the inoculant particles than Al melt. Strong sedimentation of the particles at the bottom of the solidified CP-Al ingot has been observed after 4 hours of holding (Figures 2 and 6). This is in good agreement with the previous studies by Gazanion *et al.*<sup>[27]</sup> and Schaffer *et al.*<sup>[13]</sup>.

It has been shown that most of the agglomerated  $TiB_2$  particles distribute along grain boundaries. This must be attributed to the grain structure development. During the settling process, some of the  $TiB_2$  particles may agglomerate together. However, agglomeration also happens during the solidification process. Once a grain refiner particle has nucleated an aluminum grain, the adjacent  $TiB_2$  particles will not be able to nucleate new grains anymore due to the reduced undercooling in the surrounding melt<sup>[9,28]</sup> caused by solute segregation. As the aluminum grain grows, only a small fraction of the neighbor particles can be gulped by the dendrite arms,

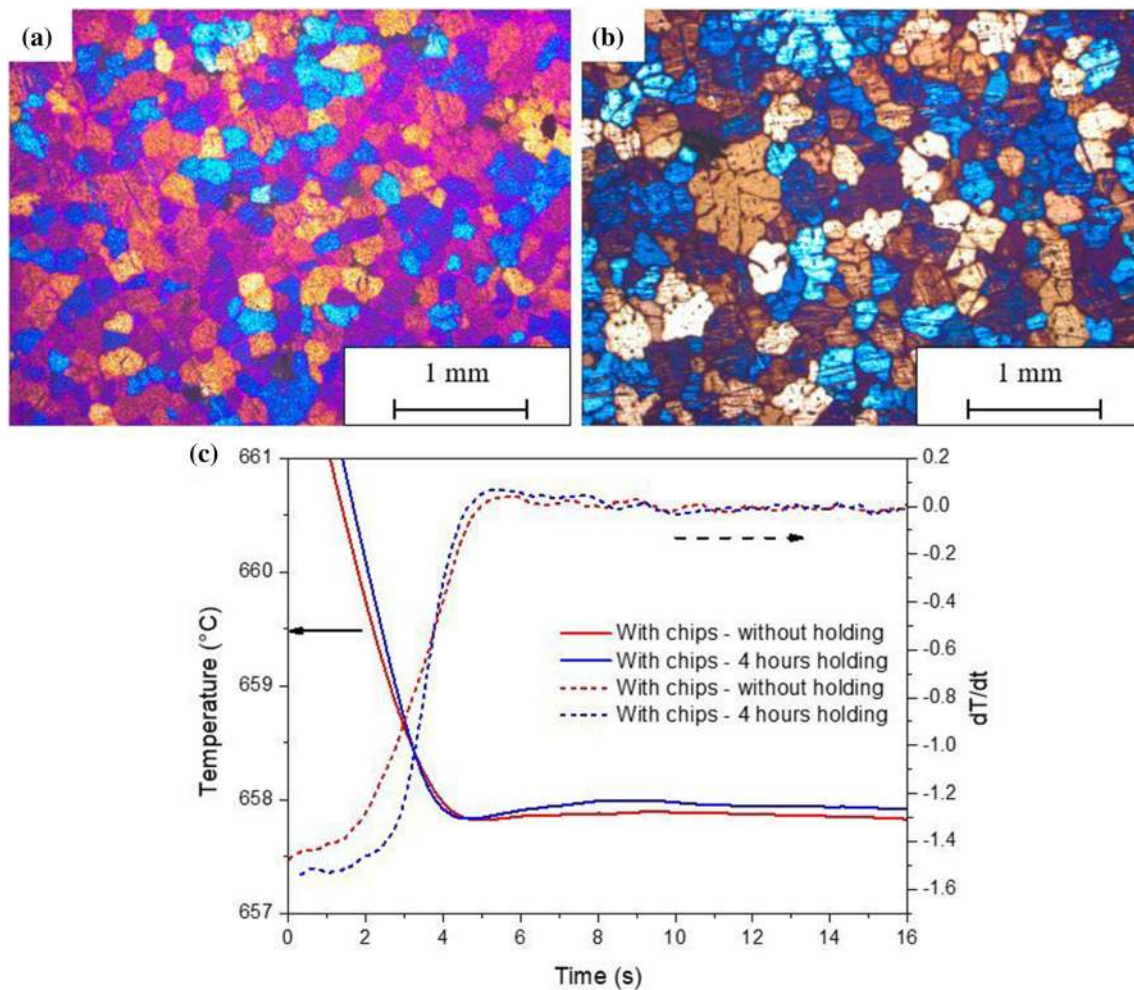


Fig. 8—Grain structure and cooling curves of TP-1 test samples of CP-Al with the addition of 6061 chips, alumina, and 10 g/kg Al-3Ti-1B. (a) sample C, solidified immediately after the addition of grain refiners (b) sample D, solidified after 4 h of holding of the inoculated melt at 750 °C. (c) The cooling curve (solid lines) with the corresponding first derivative  $dT/dt$  (dashed lines) of Samples C and D.

while the majority will be pushed to the solidification front by the dendrite arms. In the late stage of solidification, they all agglomerate at the grain boundaries in connection with eutectic Al-Fe intermetallic particles, forming structures as shown in Figures 2(c) and (d). This is the so-called solidification frontline accumulation. Meanwhile,  $TiB_2$  clusters also form in the intragranular regions as shown in Figure 3(e). This is an evidence that the  $TiB_2$  particles may have agglomerated with each other in liquid aluminum before they are pushed to the solidification front. An agglomeration of the particle is supposed to reduce the total surface energy of the particles.

It is interesting to see that the addition of 6061 chips has significantly alleviated the sedimentation of  $TiB_2$  particles and alumina particles. Even after 4 hours of holding time, the amount of settled  $TiB_2$  particles at the bottom section is significantly reduced, as shown in Figures 6(b) and (d). By further magnifying Figure 3(d), Figure 9 shows typical hexagon-shaped  $TiB_2$  particles tangled by oxide film.  $TiB_2$  in chain or as clusters are

attaching to both sides of the oxide films. These clusters may be caught by the films as a whole piece or they may have agglomerated by attracting new individual  $TiB_2$  particles during settling. Furthermore, some  $TiB_2$  particles are also found to be embedded in between oxide films. This may be similar to the formation of bi-films. In this case, not only aluminum melt and gas but also grain refiner particles were wrapped inside the films.<sup>[29]</sup> This is different from the CP-Al melt without chip addition, where no  $TiB_2$  was found at the top region after 4 hours of settling. It is suggested that a strong adherence exists between  $TiB_2$  particles and oxide film, which prevents the sedimentation of grain refiner particles. This supports our previous research on the wetting behavior of Al-3Ti-1B master alloy on alumina substrate,<sup>[23]</sup> where the  $TiB_2$  particles are found to adhere to the oxide skin of aluminum droplets periphery. The strong adherence of  $TiB_2$  particles to oxide films has reduced the number of particles that can sediment freely in the melt. On the other hand, no direct strong adherence between oxide particles and  $TiB_2$  particles was observed.



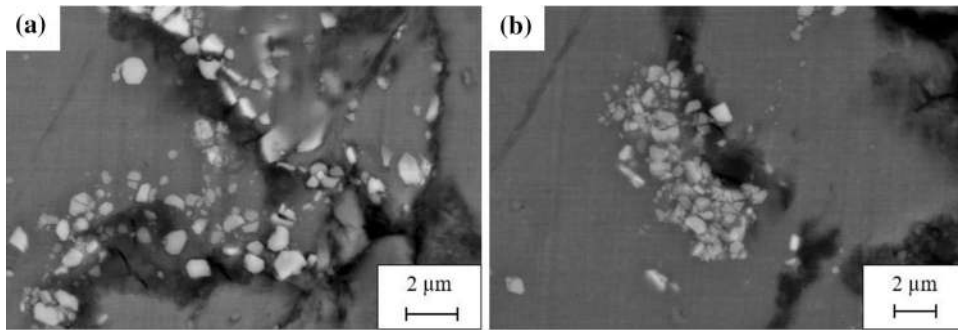


Fig. 9—Interaction between  $\text{TiB}_2$  particles and oxide films in Sample C, by the magnification of Fig. 3(d). (a)  $\text{TiB}_2$  particles (bright) attached to oxide films (dark). (b)  $\text{TiB}_2$  particles adhere to the bottom side of oxide films.

Figure 7 has shown that 4 hours of settling has significantly reduced the grain refinement effect of the alloy, although a high amount of grain refiners were added. This is owing to the fading effect of grain refiners caused by sedimentation and agglomeration of  $\text{TiB}_2$  particles during long-time holding of the inoculated melt. The sedimentation of  $\text{TiB}_2$  particles to the bottom of the crucible leads to a heterogeneous distribution of potential nucleation particles in the melt as shown in Figure 6(b). The agglomeration of the particles will significantly reduce the number density of potent nucleation particles. One of the  $\text{TiB}_2$  particles in the agglomeration has initiated an aluminum grain, a solute segregation zone will form around this grain, and then the other  $\text{TiB}_2$  particles are not able to initiate new grains due to the solute-suppressed nucleation (SSN) effect.<sup>[9,30]</sup> Interestingly, it is found that an introduction of a large amount of aluminum oxide films in aluminum melt can significantly reduce the settling of grain refiner particles due to the strong adherence of  $\text{TiB}_2$  particles on the oxide films floating in the melt. On the other hand, the adhering of  $\text{TiB}_2$  particles on oxide films also retard the floating up of oxide films due to the higher density  $\text{TiB}_2$  particles than aluminum melt. Although a large fraction of the grain refiner particles, mostly adhering to the oxide films, are remained in the upper part of the melt in the furnace, after 4 hours of holding, the grain refinement efficiency is still reduced, as shown in Figure 8. This can be attributed to the very small distance among particles adhered to the surface of oxide films, where only a small fraction can nucleate aluminum grains. Furthermore, if  $\text{TiB}_2$  particles are wrapped into the films as shown in Figure 9(a), they cannot nucleate aluminum grains either. Nevertheless, the existence of a large amount of aluminum oxide films seems to slightly alleviate the fading effect of grain refiners during long-time holding.

### B. Settling Behavior of Oxide Films and Grain Refiner Particles

To quantitatively address the influence of oxide films on the settling behavior of grain refiner particles, Stokes' law has been applied to calculate the terminal velocity  $v$  of particles and drag force  $F_D$  exerted on spherical

objects by the viscosity of melt. With small Reynolds numbers in a viscous fluid, such as static test in present work,  $v$  and  $F_D$  can be expressed as

$$v = \frac{2r^2(\rho_p - \rho_f)g}{9\mu} \quad [1]$$

$$F_D = 3\pi\mu vd \quad [2]$$

In the equations,  $r$  is the radius of the spherical particle (cm);  $\rho_p$  is the density of particles, which is 4.5 and 3.97 g cm<sup>-3</sup> for  $\text{TiB}_2$  and  $\text{Al}_2\text{O}_3$ , respectively<sup>[31,32]</sup>;  $\rho_f$  is the density of liquid Al (2.345 g cm<sup>-3</sup>) at 751 °C<sup>[33]</sup>;  $g$  is the acceleration due to gravity (980 cm s<sup>-2</sup>); and  $\mu$  is the viscosity of liquid Al (0.01126 g/(cm s)) at 751 °C.<sup>[33]</sup>

The settling velocity of particles has been calculated based on the following assumptions:

1. No initial force was acting on particles except for gravity.
2. The morphology of the particles is spherical and has a diameter in the range of 1 to 10  $\mu\text{m}$ .
3. The only drag force considering is the force between melt and particles, the wall effect and thermal gradient convection effect have been ignored.

The times needed to travel 4.5 cm distance (total height of the aluminum melt in the crucible) for a spherical particle with a size of 0 to 10  $\mu\text{m}$  are shown in Figure 10. Heavy  $\text{TiB}_2$  particles settle faster than  $\text{Al}_2\text{O}_3$  particles. With agglomeration, grain refiner particles settle even faster than what is predicted by Stokes' law.<sup>[14]</sup> It shows that after 4 hours of holding, all the particles larger than 1  $\mu\text{m}$  can be sedimented at the bottom of the crucible. This fits well with experimental observations: no  $\text{TiB}_2$  particles are found in the top section after 4 hours of holding. But,  $\text{TiB}_2$  particles were found in the top section after 4 hours of holding when oxide films were introduced. Therefore, the shape factor of the grain refiner particles must be considered in order to address the settling of grain refiner particles adhered to the oxide films.

The shape factor of films plays an important role during the settling of films and it can be described by the drag coefficient ( $C_D$ ). The drag force of the particle is

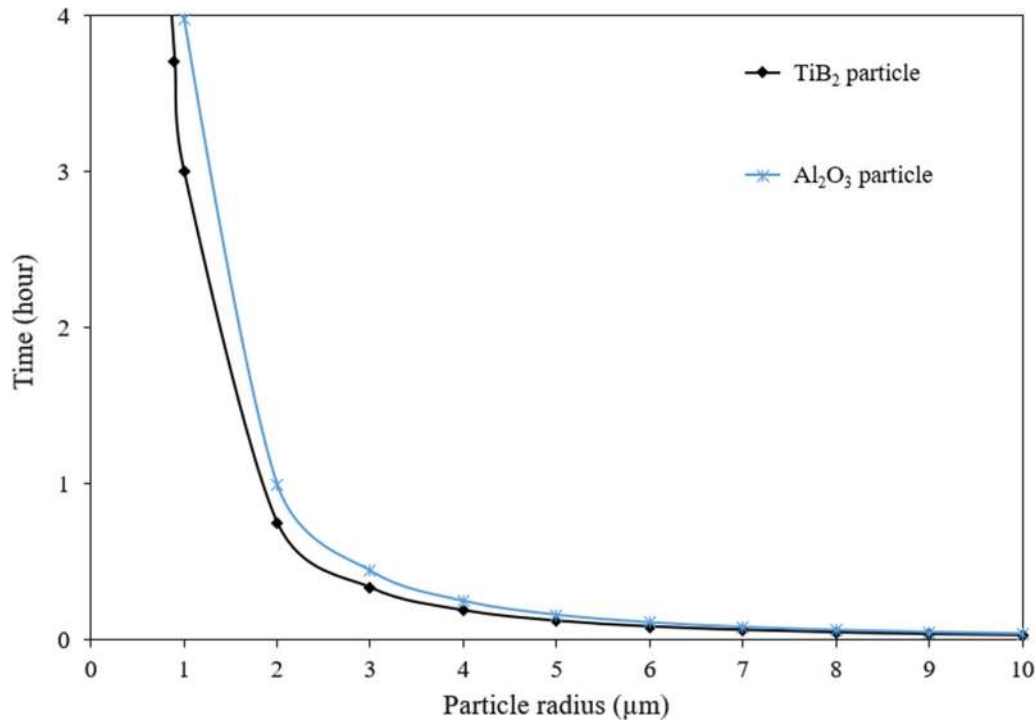


Fig. 10—Calculated time needed for TiB<sub>2</sub> and alumina particles in Al melt at 751 °C to settle 4.5 cm distance down to the bottom of the crucible, as a function of particle radius.

determined by this coefficient through Eq. [3], and it can change the particle velocity during settling in a fluid.<sup>[34]</sup>

$$F_D = \frac{1}{2} \rho_f v_f^2 C_D A, \quad [3]$$

where A is the surface area of the particle. Due to the difference in C<sub>D</sub>, the terminal velocity of a thin film will be different from an alumina particle although their density is identical. By an approximation of thin disc geometry, the terminal velocity of a thin film can be described as follows<sup>[16,34,35]</sup>:

$$v_{oxidefilm} = \frac{(\rho_p - \rho_f) \pi d t g}{32 \mu}, \quad [4]$$

where t is the thickness of the disc (cm) and d is the diameter of the particle (cm).

Figure 11 shows the terminal velocity of Al<sub>2</sub>O<sub>3</sub> particle, TiB<sub>2</sub> particle, aluminum oxide films, and oxide films with an adhered TiB<sub>2</sub> particle in aluminum melt. When calculating the terminal velocity of films with adhered TiB<sub>2</sub> particles, the resulting density is assumed to be the weight-averaged densities of both particles. Yet, the morphology remains the same as the film. As can be seen, the terminal velocity of TiB<sub>2</sub> particles is significantly reduced when they are adhered to oxide films. This calculation fits well with the settling experimental observation. Moreover, if the oxide films remain thin in thickness, the terminal velocity is then not very dependent on the disc diameter. It has to be noted that the floating behavior of oxide films cannot be explained by the current calculation. The floating of oxide films

may be attributed to the formation of folded oxide films,<sup>[29]</sup> where some gas is entrapped between the oxide films. These give an extra buoyancy force for oxide films to float up.

## V. CONCLUSIONS

In the present work, the interactions between aluminum oxide films and TiB<sub>2</sub> particles in aluminum melt during settling and their effects on the grain refinement behavior have been studied. The major findings can be summarized as the following:

1. There is a strong tendency for the TiB<sub>2</sub> particles to agglomerate and settle in aluminum melt during melt holding. Most of the grain refiner particles are sedimented in the bottom of the crucible and agglomerated along grain boundaries in the solidification structure.
2. An introduction of oxide films in aluminum melt can significantly reduce the sedimentation of TiB<sub>2</sub> particles. A large fraction of the grain refiner particles in forms of chains or clusters are found adhering to aluminum oxide films distributed at the top part of the aluminum melt. This is due to the dragging force of oxide films on the TiB<sub>2</sub> particles in the melt.
3. Grain size measurement and cooling curve study of TP-1 type solidification tests show that the grain refinement efficiency is significantly reduced by a long-time holding of inoculated aluminum melt, regardless of the inclusion level in the melt. However,

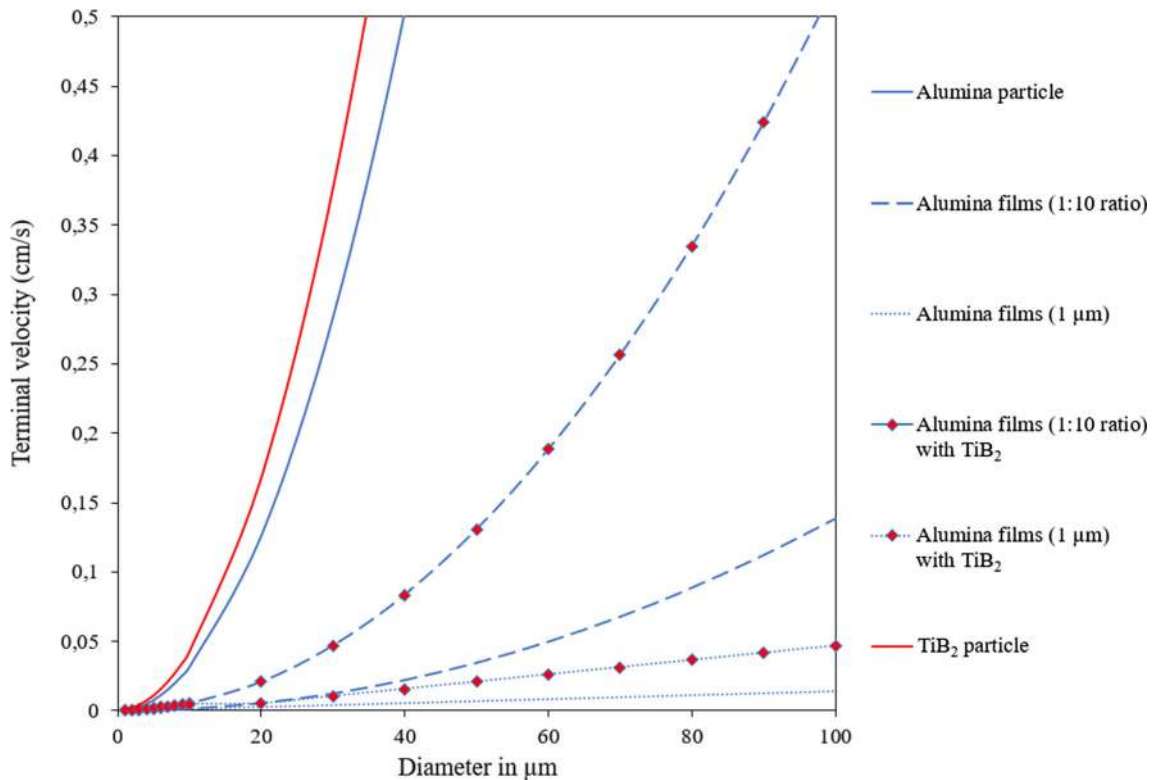


Fig. 11—Calculated terminal velocity of the particle (solid line), the film with a thickness-to-diameter ratio of 1:10 (dashed line), and film with a constant 1  $\mu\text{m}$  thickness (dotted line). Oxides based on Stokes' law with the addition of  $\text{TiB}_2$  (marked with diamond). The blue color is for  $\text{Al}_2\text{O}_3$ , the red color is for  $\text{TiB}_2$  particle. 1  $\mu\text{m}$  refers to the film thickness, and 1:10 refers to thickness:particle diameter ratio (Color figure online).

it seems that the introduction of a large amount of aluminum oxide films can slightly alleviate the fading effect of grain refiners over holding time. This is attributed to the strong adherence between  $\text{TiB}_2$  particles to oxide films, which retards the sedimentation of the particles.

- The oxide powders do not show any direct strong interaction with  $\text{TiB}_2$  particles, and therefore have little influence on the sedimentation behavior of  $\text{TiB}_2$  particles.

#### ACKNOWLEDGMENTS

This research was carried out as part of the BIA-IPN Project (256724/O20) SmartAl, funded by Norwegian Research Council (NRC). It includes the following partners: Hydro Aluminum AS, Hydal Aluminum Profiler AS, Hycast AS, Ekornes ASA, NTNU, and SINTEF. Funding by the industrial partners and NRC is gratefully acknowledged.

#### FUNDING

Open access funding provided by NTNU Norwegian University of Science and Technology (incl St. Olavs Hospital - Trondheim University Hospital).

#### OPEN ACCESS

This article is licensed under a Creative Commons Attribution 4.0 International License, which permits use, sharing, adaptation, distribution and reproduction in any medium or format, as long as you give appropriate credit to the original author(s) and the source, provide a link to the Creative Commons licence, and indicate if changes were made. The images or other third party material in this article are included in the article's Creative Commons licence, unless indicated otherwise in a credit line to the material. If material is not included in the article's Creative Commons licence and your intended use is not permitted by statutory regulation or exceeds the permitted use, you will need to obtain permission directly from the copyright holder. To view a copy of this licence, visit <http://creativecommons.org/licenses/by/4.0/>.

#### REFERENCES

- D.G. McCartney: *Int. Mater. Rev.*, 1989, vol. 34 (1), pp. 247–60.
- B. Murty, S. Kori, and M. Chakraborty: *Int. Mater. Rev.*, 2002, vol. 47 (1), pp. 3–29.
- I. Naglič, A. Smolej, M. Doberšek, and P. Mrvar: *Mater. Charact.*, 2008, vol. 59 (10), pp. 1458–65.
- R.-G. Guan and D. Tie: *Acta Metall. Sin. (English Letters)*, 2017, vol. 30 (5), pp. 409–32.

5. A. Greer, A. Bunn, A. Tronche, P. Evans, and D. Bristow: *Acta Mater.*, 2000, vol. 48 (11), pp. 2823–35.
6. I. Maxwell and A. Hellawell: *Acta Metall.*, 1975, vol. 23 (2), pp. 229–37.
7. Q. Du and Y. Li: *Acta Mater.*, 2014, vol. 71, pp. 380–89.
8. Z. Fan, Y. Wang, Y. Zhang, T. Qin, X.R. Zhou, G.E. Thompson, T. Pennycook, and T. Hashimoto: *Acta Mater.*, 2015, vol. 84, pp. 292–304.
9. Y. Xu, D. Casari, R.H. Mathiesen, and Y. Li: *Acta Mater.*, 2018, vol. 149, pp. 312–25.
10. P. Schumacher, A. Greer, J. Worth, P. Evans, M. Kearns, P. Fisher, and A. Green: *Mater. Sci. Technol.*, 1998, vol. 14 (5), pp. 394–404.
11. C. Limmaneevichitr and W. Eidhed: *MaterSci. Eng. A*, 2003, vol. 349 (1), pp. 197–206.
12. H. Chen, J. Jie, K. Svyrenenko, H. Ma, and T. Li: *J. Mater. Res.*, 2014, vol. 29 (15), pp. 1656–63.
13. P.L. Schaffer and A.K. Dahle: *Mater. Sci. Eng. A*, 2005, vols. 413–414, pp. 373–78.
14. G.S. VinodKumar, B.S. Murty, and M. Chakraborty: *Int. J. Cast Met. Res.*, 2010, vol. 23 (4), pp. 193–204.
15. C. Tian, G.A. Irons, and D.S. Wilkinson: *MetallMater. Trans. B*, 1999, vol. 30 (2), pp. 241–47.
16. M. Badowski, M. Gökelma, J. Morscheiser, T. Dang, P. Le Brun, and S. Tewes, *Light Metals 2015*, M. Hyland, Editor. 2016, Springer International Publishing: Cham. p. 967–72.
17. C. Conti and P. Netter: *Sep. Technol.*, 1992, vol. 2 (1), pp. 46–56.
18. Whiteley, P.R., *Aluminium Cast House Technology (Seventh Australasian Conference)*. 2002, Somerset, UNITED STATES: Wiley.
19. N. Towsey, W. Schneider, H.-P. Krug, A. Hardman, and N.J. Keegan: Impact of grain refiner addition on ceramic foam filter performance, in *Continuous Casting*, K. Ehrke and W. Schneider, eds., Wiley-VCH Verlag GmbH & Co KGaA, New York, 2006, pp. 26–32.
20. N. Towsey, W. Schneider, H.-P. Krug, A. Hardman, and N.J. Keegan: *The influence of grain refiners on the efficiency of ceramic foam filters*, in *Essential Readings in Light Metals: Volume 3 Cast Shop for Aluminum Production*, J.F. Grandfield and D.G. Eskin, eds., Springer International Publishing, Cham, 2016, pp. 291–295.
21. H. Duval, C. Rivière, É. Laé, P. Le Brun, and J.-B. Guillot: *Metall. Mater. Trans. B*, 2009, vol. 40, p. 233.
22. S. Ray, B. Milligan, and N. Keegan: *Aluminium Cast House Technology*, Wiley, New York, 2005, pp. 1–12.
23. Yang J, Bao S, Akhtar S, Shen P, Li Y (2020) *Metall. Mater. Trans. B*, 2020.
24. Yang, J., S. Bao, S. Akhtar, and Y. Li, *Study of Controllable Inclusion Addition Methods in Al Melt*. 2019. p. 1041–48.
25. Y. Xu, Y. Deng, D. Casari, R.H. Mathiesen, X. Liu, and Y. Li: *J. Mater. Sci.*, 2020, vol. 55 (32), pp. 15621–635.
26. Aluminum Association : *Standard test procedure for aluminum alloy grain refiners*, Aluminum Association, Arlington, 2012.
27. F. Gazanion, X.G. Chen, and C. Dupuis: *Mater. Sci. Forum.*, 2002, vol. 396, pp. 45–52.
28. Y. Xu, D. Casari, Q. Du, R.H. Mathiesen, L. Arnberg, and Y. Li: *Acta Mater.*, 2017, vol. 140, pp. 224–39.
29. J. Campbell: *J. Mater. Sci.*, 2016, vol. 51 (1), pp. 96–106.
30. D. Shu, B. Sun, J. Mi, and P.S. Grant: *Acta Mater.*, 2011, vol. 59 (5), pp. 2135–44.
31. N.V. Buchilin, V.G. Maksimov, and V.G. Babashov: *Glass Ceram.*, 2015, vol. 72 (7), pp. 246–52.
32. C. Baron and H. Springer: *Data in Brief*, 2017, vol. 12, pp. 692–708.
33. M.J. Assael, K. Kakosimos, R.M. Banish, J. Brillo, I. Egry, R. Brooks, P.N. Quested, K.C. Mills, A. Nagashima, and Y. Sato: *J. Phys. Chem. Ref. Data*, 2006, vol. 35 (1), pp. 285–300.
34. G. Ahmadi: *Proc. ME*, 2003, vol. 437, pp. 1028–40.
35. M. Gökelma, P. Le Brun, T. Dang, M. Badowski, J. Morscheiser, B. Friedrich, and S. Tewes: *Assessment of settling behavior of particles with different shape factors by LiMCA data analysis*, in *Light Metals 2016*, E. Williams, ed., Springer International Publishing, Cham, 2016, pp. 843–48.

**Publisher's Note** Springer Nature remains neutral with regard to jurisdictional claims in published maps and institutional affiliations.